Available online at www.sciencedirect.com
ScienceDirect
Journal of Power Sources 163 (2006) 440–449
JOURNAL OF POWER SOURCES
www.elsevier.com/locate/jpowsour

# Development and performance analysis of a $H_2$/air micro PEM fuel cell stack

Shou-Shing Hsieh *, Chih-Lun Feng, Ching-Feng Huang

*Department of Mechanical and Electro Mechanical Engineering, National Sun Yat-Sen University, 80424 Kaohsiung, Taiwan, ROC*

Received 12 July 2006; received in revised form 31 August 2006; accepted 15 September 2006
Available online 27 October 2006

**Abstract**

Research and development was conducted on a $H_2$/air micro proton exchange membrane (PEM) fuel cell stack to investigate the polarization curves under different operating conditions, such as temperature, pressure, and humidification of the $H_2$ gas streams. A novel design of copper metal bipolar plates (BPs) was developed as well as fabricated in-house and used in this fuel cell stack. The performance of the stack was tested and the methodology as well as associated technology found to be promising for the first time on micro PEM fuel cell stack with an innovative bipolar plate design and fabrication.


*Keywords:* Micro PEM fuel cell stack; Innovative bipolar plate; Microfabrication; Stack performance

## 1. Introduction

The use of microfabrication technology for fulfillment of power generation has ever been increased with being widely and generally demanded in portable electronic applications especially for 3C products. One of the notable and promising examples is micro fuel cell system, for instance, micro PEM fuel cell/or micro direct methanol (DM) fuel cell, which is now target for battery replacements for portable electronic devices and miniature power source. In general, the fuel cells produce between 30 mW (single cell) and 500 mW (cell stack) of power [1–3]. In fact, micro fuel cells are expected to attain higher energy density than that of a lithium ion battery by converting hydrocarbon fuel to electric power at several percentage or higher efficiency.

A miniaturized fuel cell power source can be considered as an approach that combines thin film materials with micro-electro-mechanical system (MEMS) technology. Micro fuel cells as mentioned before, which generate less than 5 W electricity for a single cell are generally developed either by silicon/polymeric micro machinery with current collectors normally embedded in the flow channels [1,2,4]. Although few papers dealt with micro fuel cells in both PEM/and DM fuel cells, very few papers have reported work on micro fuel cell stacks in either PEM/or DM fuel cell stack.

The present study has developed/fabricated in-house an innovative micro proton exchange membrane (PEM) fuel cell stack with a new/novel bipolar plate design. Performance tests were conducted through a series of laboratory experiments with different operating conditions of temperature, pressure as well as humidification of the $H_2$ gas streams.

For a fuel cell stack with series connected single cells, operating conditions may vary significantly not only in the plane of the MEA but also along the stack axis. The effect and influence would be totally different from that operated in a single cell. In fact, an even fluid distribution to all the individual cells and a homogenous temperature distribution are difficult to achieve [6]. Such an examination of operating parameters on polarization curves is essential and necessary.

The objective of this study was to complement/advance our previous work from a single cell of micro PEM fuel cell [1,2,5] to a fuel cell stack in both fabrication technique and performance demonstration. Salient feature of micro PEM fuel cell stack technology was examined, including the BPs material selection, operating conditions (stack temperature, anode back-pressure and humidification of the $H_2$ gas streams) on stack performance, and stack reactant feed configurations.

* Corresponding author. Tel.: +886 7 5252000x4215; fax: + 886 7 5254215.
*E-mail address:* sshsieh@mail.nsysu.edu.tw (S.-S. Hsieh).

0378-7753/$ – see front matter © 2006 Elsevier B.V. All rights reserved.
doi:10.1016/j.jpowsour.2006.09.027

## 2. Experimental

Major development activities [7] were focused on the microfabrication of cell stack including bipolar plates design and fabrication assembling/bonding cell stack, and performance test of entire cell stack.

### *2.1. Copper (Cu) electroforming bipolar plates (BPs)/end plates*

As stated previously, the applications of fuel cell to portable power is motivated by numerous occasions, such as 3C products (communication, computing, camcorder) and challenged by several factors, for example, high power density and high energy to weight ratio. For micro PEMFCs to become a commercial reality as cell stacks, a lot of work needs to be done [5]. One of major issues concerned is the bipolar plates material selected and fabrication technique used for a PEM fuel cell stack.

The BPs were designed based on the stacking concept where all the components of the micro fuel cell are layed in a stack and fabricated to achieve the demands as stated previously. The materials that BPs are made of would have different physical and chemical properties related to each functions. Therefore, it is extremely difficult to find a material to qualify all the major requirements mentioned above. Although metal plates have plenty of aforementioned merits, they are prone to corrosion or dissolution. The dissolved metal ions may lead to poisoning of PEM membrane and hence lowering of ionic conductivity. Consequently, these impede cell stack performance. For those used/considered metal plate materials, copper is seldom to be mentioned. This is perhaps because it has a comparable high weight and has more corrosive. Despite of these deficiencies of copper material, the present study would like to examine its superiority carefully and quantitatively based on the operating condition, which might provide a different thinking and an alternative as far as BPs material selection is concerned. In fact, the present study is for micro PEM fuel cell stacks of which their working condition most likely is less than 70 °C and the presence of gas diffusion layer (GDL), which can also acted as a passivating layer. All of these can be considered as protection strategy to avoid the Cu bipolar plates cell stacks operating under a harsh environment (e.g. acid solution, relative high temperature, etc.). Table 1 lists the relevant comparison among these potential BPs materials including cost estimate. The value shown in Table 1 indicates Cu metal can be more saved up to one fifth of that of graphite plate.

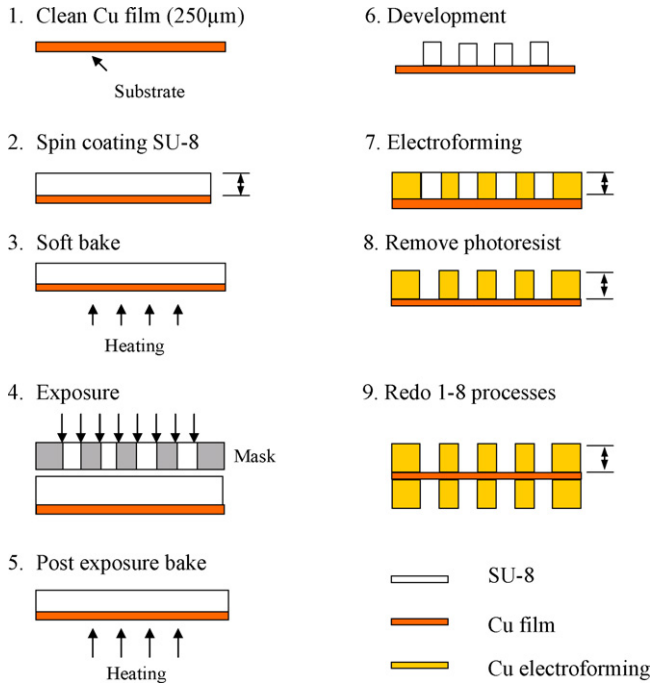


Fig. 1. Microfabrication processes of bipolar plate.

In view of the above discussion, copper metals, as sheets, were thus used to make bipolar plates by using LIGA-like microfabrication process of deep UV lithography to obtain SU-8 (2100) resist patterns/and SU-8 mould. Fujifilm transparency (HPB7S) designs were created and used as masks in contact photolithography to yield master. Using transparencies printed from high resolution printer, we can rapidly and reliably create features in photoresist with width $\geq$15 μm for the associated flow channels in bipolar plates. Through electroforming process, the patterned SU-8 channel structure, 200 μm depth, 300 μm width with a 150 μm rib, was electroplated in a copper sulfa mate bath using direct current (dc) at a current density 20 mA cm$^{-2}$. Redo the processes again, Cu bipolar plates/end plates with serpentine (meander) flow channels well thus obtained. Detailed fabrication steps in sequence and fabrication parameters and operating conditions are shown in Fig. 1 and given in Table 2, respectively,

Table 1
Properties of several bipolar plate materials at 300 K

| | Graphite (commercial) | Stainless steel (SS316) | Copper | Nickel |
|---|---|---|---|---|
| Thermal conductivity (W mK$^{-1}$) | 25–80 | 15.9 | 401 | 90.7 |
| Electrical conductivity (S m$^{-1}$) | $2 \times 10^5$ | $1.35 \times 10^6$ | $8.7 \times 10^7$ | $3.54 \times 10^7$ |
| Density (kg m$^{-3}$) | 1950 | 8000 | 8940 | 8900 |
| Modulus of elasticity (GPa) | 8–15 | 193 | 110 | 207 |
| Coefficient of thermal expansion ($10^{-6}$ K$^{-1}$) | 1.2–8.2 | 10–11.7 | 17 | 12.9–13.3 |
| Corrosion rate (mm year$^{-1}$) | $\leq 2.8 \times 10^{-3}$ | $\leq 10^{-2}$ | $\leq 10^{-2}$ | $\leq 10^{-2}$ |
| Gas permeability (cm$^3$ min$^{-1}$ cm$^{-2}$) | $0.8–2 \times 10^{-5}$ | $\leq 10^{-6}$ | $\leq 10^{-6}$ | $\leq 10^{-6}$ |
| Specific heat (J kg$^{-1}$ K$^{-1}$) | 710–830 | 420–500 | 386 | 456 |
| Cost (NTD* kg$^{-1}$) | 1025 | 160–200 | 190 | 170–200 |
| Poisson's ratio | 0.1–0.29 | 0.3 | 0.34 | 0.31 |

* NTD: new Taiwan dollar.

Table 2
Fabrication parameters and conditions

| | |
|---|---|
| PR coating | SU-8 2100 |
| PR property | Negative |
| PR type | Thick film |
| Dehydration bake (°C) | 150 |
| Speed (rpm) | 400 (40 s); 700 (60 s) |
| Soft bake (95 °C) (min) | 70 |
| UV light wave length (nm) | 365 |
| Light intensity (mW cm$^{-2}$) | 33 |
| Exposure time (s) | 75 |
| Post exposure bake (95 °C) (min) | 17 |
| Development (min) | 3 |
| Hard bake (95 °C) (min) | 5 |
| Electroforming solution | Copper sulfate, $H_2SO_4$ solution |
| Solution pH | 4 |
| Solution temperature (°C) | 31.6 |
| Current density (mA cm$^{-2}$) | 20 |
| Photoresist remover | Remover propylene glycol |

and the results are shown in Fig. 2 for the BPs configuration and 3-D image.

### 2.2. Stack configuration

To meet our power requirement, the stack design selected had the following configuration:

- small stack (2 cells) and large stack (7 cells);
- 5 cm$^2$ active area;
- commercial Pt on carbon anode/cathode catalyst;
- serpentine flow channel ($H_2$/air) with an innovative bipolar plate design and fabrication (Cu microelectroforming);
- Cu microelectroforming end plates.

All stacks were designed and built in-house. It was a 2-cell/7-cell stack with an active area of 5 cm$^2$. The flow field plates consisted of a serpentine (meander) flow pattern electroplated into a copper plate (i.e., BPs). The anode was operated with a series flow pattern, meaning the effluent from cell 1 is the inlet to cell 2, the effluent from cell 2 is the inlet to cell 3, etc. This series flow pattern ensured that anode side reactant distribution would not affect the experimental results. The cathode reactant inlet was distributed in parallel with individual side exhausts. There is no internal cooling or humidification in this system.

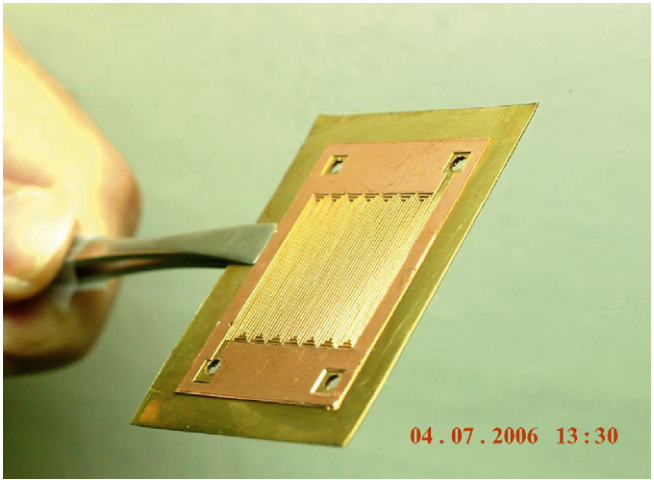


Fig. 2. Three-dimensional image of electroforming bipolar plate.

### 2.3. Fuel cell system and $H_2$/air circulating loop

The computer controlled fuel cell system and circulating loop is designed (see Fig. 3 for details) for operation with hydrogen and air. The fuel cell stack consists of 2/7 single cells, each with an active area of 5 cm$^2$. The MEAs in these stacks used Nation 117 (Electrochem) membrane and a platinum loading (Lynntech) of 0.5 mg cm$^{-2}$ on the anode and cathode side, respectively. Two 290 μm corbon paper (ELAT) of gas diffusion layers (GDLs) are from E-TEK gas diffusion media. The reactant gases are fed in series to the individed cells of the stack hydrogen ($H_2$) and air are conducted parallel-flow mode by three channel/eight pass (serpentine) on both the anode side and cathode side of each single cell.

Purified (99.9%) hydrogen is fed into the stack from a gas bottle through a mass flow meter, humidifier, and back-pressure valve. All of the experiments were conducted at 97, 153, and 207 kPa of hydrogen inlet pressure (see Table 3 for details), respectively. Incidentally, $H_2$ was recycled for another purpose. Ambient air is provided to the stack by a variable speed air compressor (SWAN, SVP-205) with capacity of 1–3 atm as also illustrated in Fig. 3. The air supply was controlled by a pressure regulator and varied between 97 and 207 kPa. Exhaust air is released into the environment via a back-pressure valve. Flow rates were fixed following the values listed in Table 3 for anode and cathode inlet. These parameters were controlled by a microprocessor based temperature controller and two back-pressure regulators. Current density versus voltage curves of 2-cell/7-cell stack were taken using a Gamry 4/750 potentiostat (scanning period 10 min) interfaced to a PC at constant current and recorded after the system reached a stable steady state (about 1.5 h) under the different operating conditions at a reasonable current density.

### 2.4. Experimental conditions, system control, and data acquisition

The cell stack system was tested using a test stand, also see Fig. 3 for details, which controls air and hydrogen flow rates, stack temperature, hydrogen humidification temperature, hydrogen/air back-pressure, and current draw. The stand includes a potentiostat system (Gamry, PC4/750) for fuel cell operation and data acquisition. The test allowed for generation of a polarization curve (both VI and PI curve) to compare performance. The PC control program is continuously monitoring the operating parameters and keeps all the conditions normal during the experiments running. The experiments were started with the power switch on the in-house made fuel cell stand and turning on the valves for $H_2$, $N_2$, and air supply chamber. Before running the experiments the anode was purged with $N_2$ to ensure no $O_2$ presence. Finally, set the maximum/minimum voltage and voltage increment as well as the time delay between two voltages in the Gamry PC4/750 potentiostat software. The present experiments

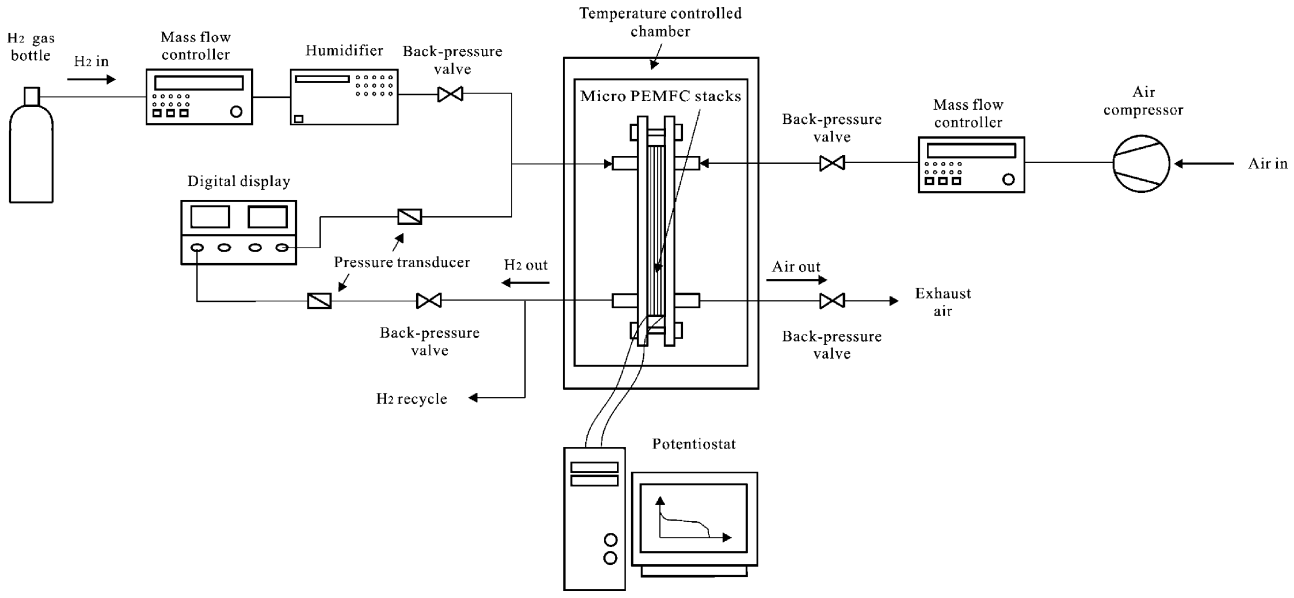


Fig. 3. Schematic of experimental apparatus.

were performed in a clean room at University Microsystem Research Laboratory. Fig. 4(a) shows a photograph of a 7-cell stack in operation. Fig. 4(b) indicates the stack lateral image of a 7-cell stack assembly.

Since this study is the first time to consider copper (Cu) as a candidate for BPs material, most results were only suitable for short term performance. For long term performance, Cu plate corrosion rate, cell stack performance decay rate, durability as

Table 3
Operating parameter and bipolar plate configuration

| | | | | |
|---|---|---|---|---|
| Inlet gas | Anode | Hydrogen (99.9%) | | |
| | Cathode | Air | | |
| Flow rate | Anode | Cell numbers ×10 sccm | | |
| | Cathode | Cell numbers ×10 sccm | | |
| Back pressure | Anode | 97kPa | 153kPa | 207kPa |
| | Cathode | Forced Air | | |
| Stack temperature | 25°C | 35°C | 50°C | |
| Anode humidifier temperature | 25°C | 35°C | 50°C | |
| Bipolar plate Channel (H×W×L) | Serpentine | 200μm× 300μm× 22.5mm | | |
| MEAs | Nafion 117 | Anode :Pt on Carbon(0.5mg/cm$^2$) | | |
| | | Cathode: Pt on Carbon(0.5mg/cm$^2$) | | |
| | GDL | Anode: Carbon Paper Based Material(290μm) | | |
| | | Cathode: Carbon Paper Based Material(290μm) | | |
| Electrode | Copper | | | |
| Active area | 5 cm$^2$ (for single cell) | | | |
| Cell numbers | 1, 2, and 7 | | | |

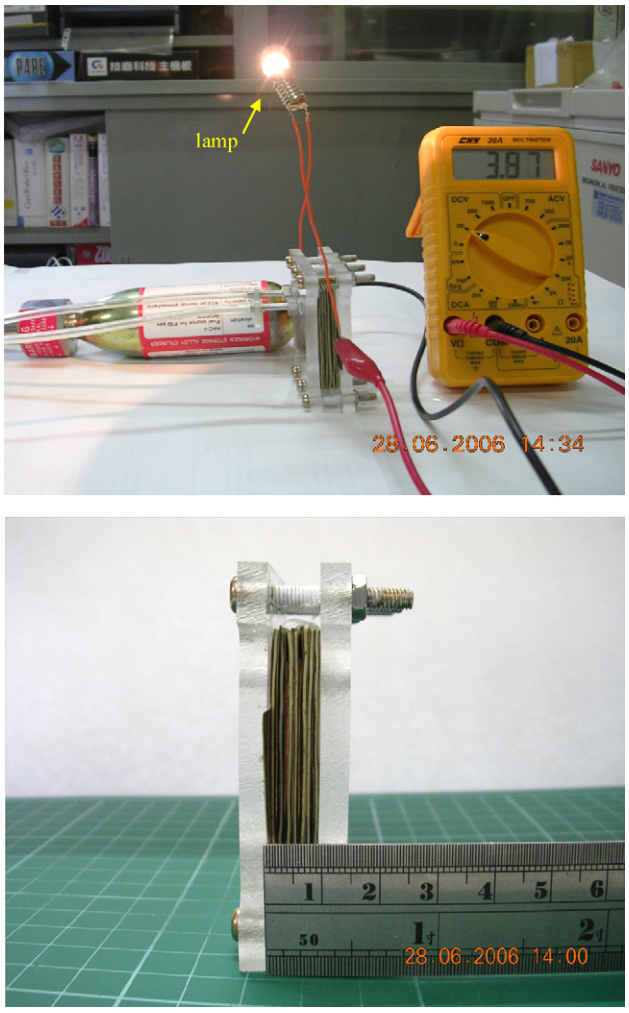


(a)

(b)

Fig. 4. Images of 7-cell stack. (a) Image for 7-cell stack during operation. (b) Lateral image of 7-cell stack.

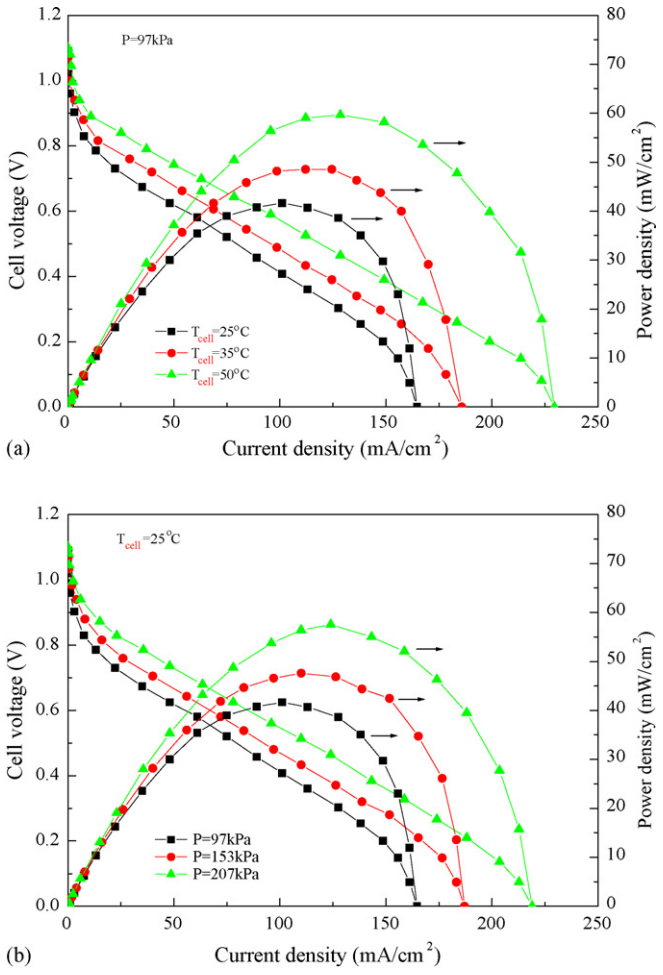


Fig. 5. The performance test for single cell. (a) Fixed anode $P = 97$ kPa and different cell temperature. (b) Fixed $T_{cell} = 25\,^{\circ}C$ and different anode pressure.

well as contamination of MEAs by copper (Cu) should be carefully examined. Further study may include these aspects.

## 3. Results and discussion

Before formal tests for cell stacks, the corresponding single cell tests with various operating conditions which can be considered as a reference to verify the consistency and validity of the present cell stack experiments were also made. One of the single cell performance results was shown in Fig. 5(a and b) at fixed anode pressure of 97 kPa and cell temperature of 25 °C, respectively, where the VI/PI curves are very similar in both trend and magnitude to one of authors' earlier work [5].

The small 2-cell stack and large 7-cell stack assembled from 2 and 7 repeated units of membrane electrolyte assembly (MEAs) and bipolar plates (including two end plates) with a thickness of 3.05 and 10.05 mm, respectively. As stated previously, the MEA is composed of two electrodes and electrolyte membrane (such as Nafion 117). The bipolar plate has many flow channels on each side designed for supply of $H_2$ and air. Electricity passes through each bipolar plate, forming electric polarization between both sides. The experiments with ambient air (relative humidity ≅ 40%) were directed to the examination of the effect of the relevant parameters of different cell operating temperatures and back-pressures of the anode with dry $H_2$/and wet $H_2$ ($T_{hum} = 25$, 35, and 50 °C) supply in serpentine channels as listed in Table 3.

### 3.1. Effect of stack operating temperature

Three operating temperature 25, 35, and 50 °C were employed to study the effect of stack operating temperature on the micro fuel cell stack. During the experiments, the $H_2$ mass flow rate for each unit cell was fixed at 10 sccm, which was found as an optimum in one of authors' papers [2]. The back-pressures on the anode were kept at 97, 153, and 207 kPa with a fixed cathode back-pressure of 97 kPa for forced air. The $H_2$ gas was humidified before entering to the anode flow channels. One of the polarization curves at the anode back-pressure of 97 kPa for each experiment was selected as a typical example, shown in Fig. 6 to illustrate such effect.

In general, the performance of PEM fuel cell stack shows a strong dependence of operating temperature. Although the

reversible potential decreases with increasing temperature, the performance actually increases due to an increase in reaction and a fast mass transfer rate with dry $H_2$ gas fed in. Meantime, because of such an increase in operating temperature, a higher rate of evaporation occurs and the reactant gases can take up more water vapor due to higher saturation pressure as stack temperature $\leq$50 °C of the present study.

It is known that the cell polarization curve is generally composed of three stages, which are concerned with the chemical activation losses, the ohmic losses, and the mass transport losses. Fig. 6(a) shows that the present 2-cell stack performance also has these three stages as the usual PEM single cell does. The open circuit voltage (OCV) was found to be about 1.9 V, and the short circuit current density at the stack temperature of 25 °C with dry $H_2$ gas was about 163 mA cm$^{-2}$. Again, the delayed transition of mass transport activation occurs at a higher current density was found like the single cell.

With operating stack temperature increase, the limiting current density can be extended to 220 mA cm$^{-2}$ at 50 °C as expected due to an ion conductivity of the ionomer increases with stack temperature. As a result, the slope of the linear portion of the curve decreases as the stack temperature increases. Simultaneously, the performance increase in terms of power density also shown in Fig. 6(a) is also based on the improved kinetics and mass transport with increasing temperatures. The trend and shape of the VI and PI curves are similar to those in conventional cell stacks. Fig. 6(b) shows the stack performance in terms of VI/PI curve for 7-cell stacks. Again, the similar trend with different stack voltage scale but the same current density level was found. However, due to non-uniformity for $H_2$/air supply conditions, the VI/PI distribution are not as smooth as that for 2-cell stack as expected. In fact, the limiting current density of 7-cell stack is a little bit smaller than that for 2-cell stacks after taking a further look. Moreover, the stacks could be dried out with time as the stack temperature increases. This would deteriorate the stack performance. Due to the present short term performance, such behavior did not happen. Further study may include this regard.

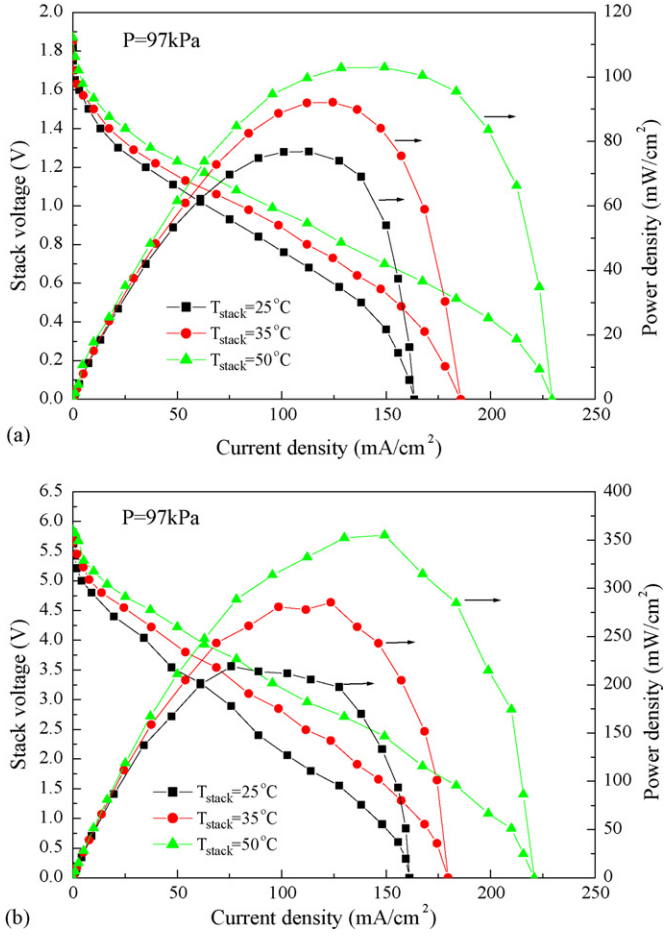


Fig. 6. The performance test for 2-cell stack and 7-cell stack at fixed anode $P$ = 97 kPa and different stack temperature. (a) 2-Cell stack. (b) 7-Cell stack.

### 3.2. Effect of anode back-pressure

The effect of the back-pressure of the flow field in the anode channels on the stack performance can be seen, as one of typical results shown in Fig. 7 with dry $H_2$ back-pressures at 97, 153, and 207 kPa, respectively, and a fixed air back-pressure at 25 °C of stack temperature for 2-cell and 7-cell stacks. Generally, a higher back-pressure would enhance the stack performance via accelerating the reaction at the both anode and cathode of the cell due to a partial pressure increase of the reactant gases. In addition, based on Nernst equation, a higher voltage can be reached at a higher pressure. Fig. 7(a) shows such trend in the VI and PI curves. It can be seen that the open circuit voltage (OCV) and the limiting current density all increase with the increase in back-pressure. Additionally, like single cell results [5], it is also found that a back-pressure increase on the anode would cause less stack performance increase than that on the cathode. This is because such a pressure drop across the membrane results in a barrier for back diffusion, which takes place to keep the membrane hydrated. Some situation and consequence were happened for 7-cell stack as depicted in Fig. 7(b). The OCV in Fig. 7(b) can reach to about 6.5 V and the maximum power density is about 325 mW cm$^{-2}$ with the current density about 125 mA cm$^{-2}$ at stack temperature of 25 °C.

### 3.3. Effect of the anode humidification

In Fig. 8(a), polarization curves with three different stack temperatures at a fixed humidification temperature are presented. Only $H_2$ stream is externally humidified with a dew temperature at 25 °C before entering the fuel cell. Generally, the VI curves shown in Fig. 8(a) have an initial rapid potential drop different from those for dry $H_2$ streams at very small current range (<10 mA cm$^{-2}$) due to electrochemical activation followed by the ohmic polarization in the remaining part of the curve. There seems no mass transport region as the conventional PEMFC and the present study for dry $H_2$ streams case does. The best stack performance was found at stack temperature of 25 °C, followed by 35 and 50 °C. The maximum stack power is about 240 mW cm$^{-2}$ at current density of 350 mA cm$^{-2}$ for $T_{stack}$ = 25 °C as also shown in Fig. 8(a).

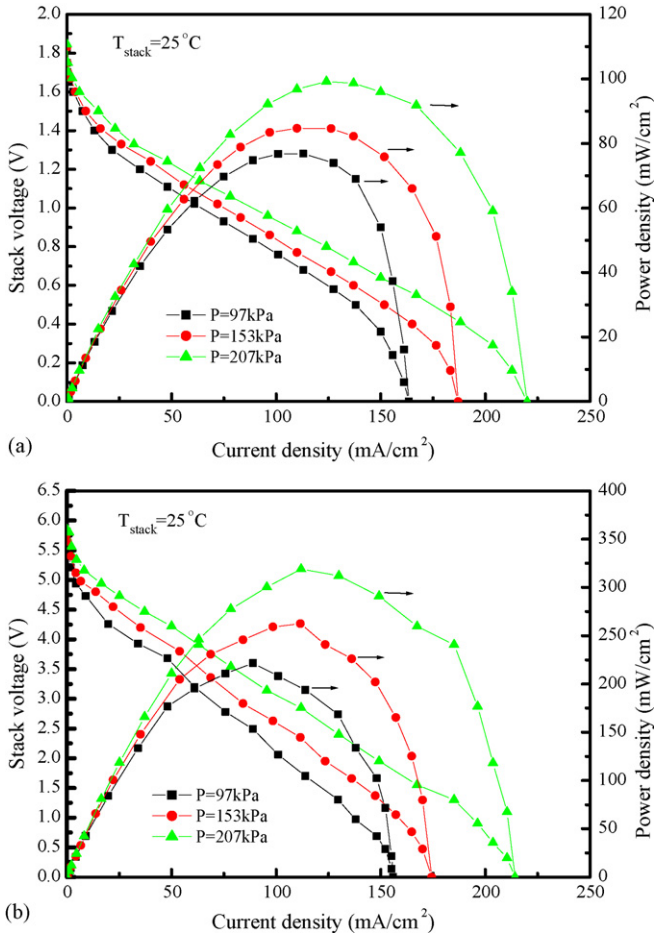


Fig. 7. The performance test for 2-cell stack and 7-cell stack at fixed $T_{stack} = 25\,^{\circ}C$ and different anode pressure. (a) 2-Cell stack. (b) 7-Cell stack.

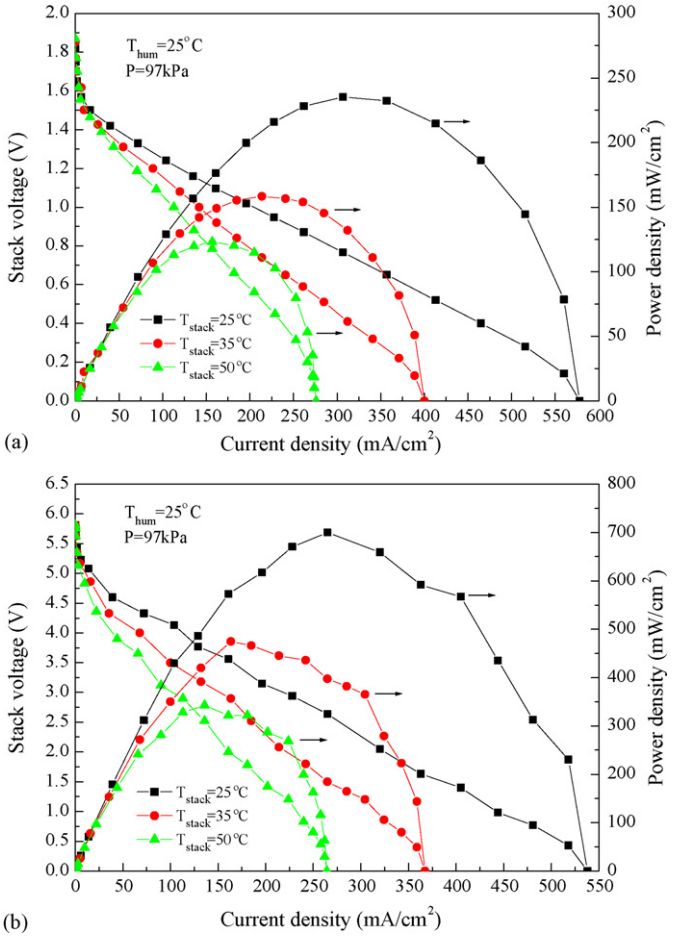


Fig. 8. The performance test for 2-cell stack and 7-cell stack at fixed $T_{hum} = 25\,^{\circ}C$, $P = 97\,kPa$ and different stack temperature. (a) 2-Cell stack. (b) 7-Cell stack.

With increasing stack temperature, the stack performance decreases. This is majorly because the drying condition occurs and slightly because the liquid block due to water vapor condensation exists in the reactant gas channel. This would deteriorate the stack performance. Of course, the stack performance of the dry $H_2$ was the worst in this case. Similarly, the same situation happens for 7-cell stacks as illustrated in Fig. 8(b) except the VI/PI curves shown in Fig. 8(b) which is not as smooth as that in Fig. 8(a).

It is obvious, from Fig. 9 that the curves do show significant temperature dependence for 2-cell and 7-cell stacks. For both Fig. 9(a and b) the stack voltage also seems to be an important parameter. The stack shows consistently best performance in terms of current density at 25 °C operating temperature for both fuel cell stacks. As operating temperature higher than 25 °C, the performance decreases which suggests dehydration, which adversely affects the ionomeric component within the catalyst layer and increases the interfacial charge resistance.

Taking a closeup examination of stack temperature, effect on current density in Fig. 9 was thus plotted against stack temperature at several stack voltage with $H_2$ stream humidification temperature at 25 °C for anode back-pressure of 97 kPa. When the stack temperature is higher than the humidification temperature, the current density decreases drastically, which indicates that the membrane is dehydrated and the active catalyst surface area may also decrease. The situation becomes less distinct as the stack voltage increases. In fact, at 1.5 V/5 V, the stack temperature effect is of no significance. Namely, at stack voltage of 1.5 V/5 V, the stack current density seems very weakly dependent on $T_{stack}$ in Fig. 9(a and b), respectively. However, this situation is gradually changed as stack voltage decreases. Generally, the current density decreases monotonically for stack voltage from 1.2 V/4 V down to 0.6 V/2.0 V. The descending rate becomes lower as $T_{stack} \geq 40\,^{\circ}C$ as evidenced in Fig. 9(a and b). Following the curves shown in Fig. 9, the maximum OCV is about 1.5 V/5.0 V and the limiting current density is about 375 mA $cm^{-2}$ at $T_{stack} = 25\,^{\circ}C$ for 2-cell and 7-cell stacks, respectively.

Fig. 10(a and b) shows the stack voltage versus stack temperature with different current density for 2-cell and 7-cell stacks, respectively. Again, the best performance was found at stack temperature of 25 °C and current density of 100 mA $cm^{-2}$. Generally, the stack voltage decreases as the current density increases at the same stack temperature. The dashed line indicates that the relative humidity of $H_2$ gases at the corresponding stack temperature of 25, 35, and 50 °C. This curve decreases

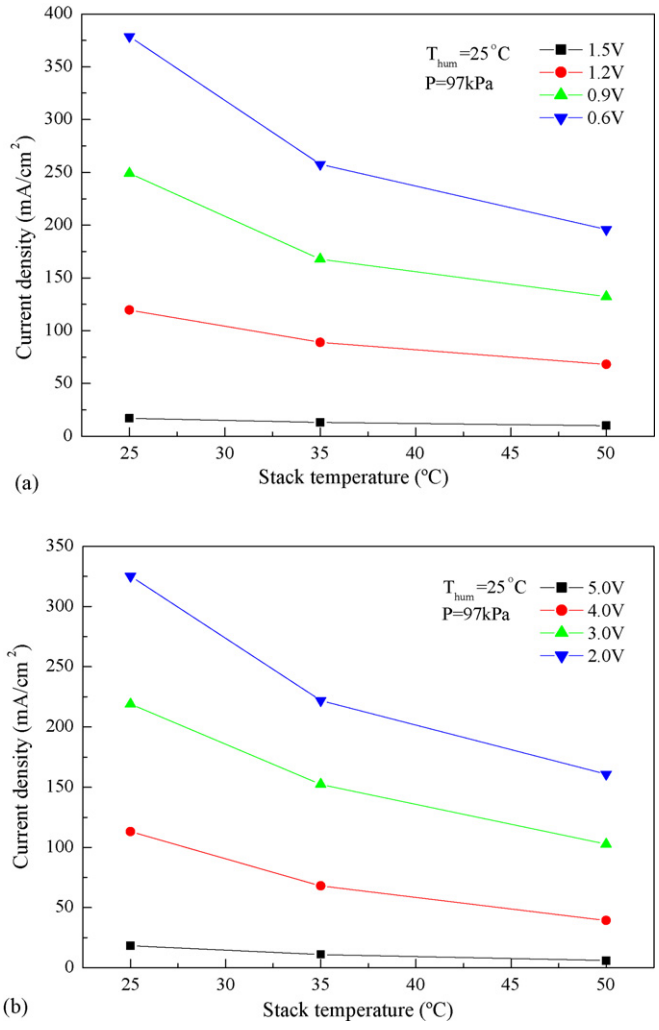


Fig. 9. Variation of current density for 2-cell stack and 7-cell stack at different stack voltage and stack temperature. (a) 2-Cell stack. (b) 7-Cell stack.

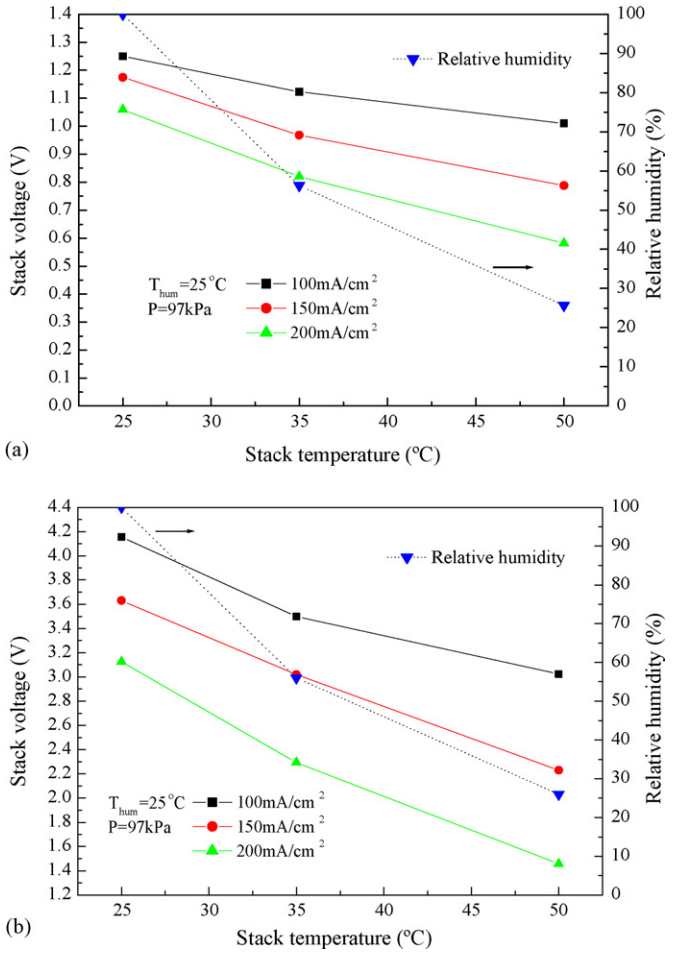


Fig. 10. Stack voltage and relative humidity as function at different stack temperature for 2-cell stack and 7-cell stack. (a) 2-Cell stack. (b) 7-Cell stack.

as the stack temperature increases because the humidification temperature of $H_2$ gases is fixed. It is can be seen that the stack temperature equals the humidification temperature of 25 °C where the relative humidity is 100% would give the best stack performance. This performance would be decreased as the relative humidity is down to 25% at stack temperature of 50 °C. When the anode becomes drying like $T_{stack} = 50$ °C in Fig. 10, the membrane becomes dehydrated which results in a stack performance depression. Again, due to membrane dehydration, the situation becomes worse at higher current density.

As stack temperature keeps at 35 °C with different gas humidification temperature of 25, 35, 50 °C at 97 kPa, the VI and PI curves show the best stack performance as noted in Fig. 11(a). The best stack limiting current density can be reached to 675 mA cm$^{-2}$ and the maximum power is about 300 mW cm$^{-2}$ at current density of 410 mA cm$^{-2}$ and $T_{hum} = 50$ °C. The VI and PI curves shown in Fig. 11(a) strongly suggested that there are two patterns on performance results. At $T_{hum} = 25$ °C, it obviously gives the lower stack performance because there seems a lower ion conductively at $T_{stack} = 35$ °C; however at $T_{hum} = 35$ and 50 °C, the membrane is nearly fully hydrated. Consequently, a higher stack performance is expected. The best performance is found at $T_{stack} = 50$ °C, which indicates that there is no observable "drying" even when the stack temperature reaches 50 °C. Again, the similar but a little bit small limiting current density (650 mA cm$^{-2}$) with an OCV about 6.0 V was found for 7-cell stack at $T_{stack} = 50$ °C as shown in Fig. 11(b).

Taking a closeup view of Figs. 11 and 12(a and b) can be deduced and plotted as current density versus anode humidifier temperature with different stack voltage for with 2-cell and 7-cell stacks, respectively. It is found that the current density increases as the $H_2$ gas humidifier temperature increases. They are two different increments as shown in Fig. 12. The rate of increase was higher in 25 °C $\leq T_{hum} \leq$ 35 °C than that in 35 °C $\leq T_{hum} \leq$ 50 °C. This is because the extent of hydration at $T_{hum} = 35$ and 50 °C seems equal and, consequently results in the curves of current density increase to be level-off (i.e., ≈constant) especially at high voltage.

Generally, the stack performance (VI/PI curves) is strongly dependent on anode back-pressure, stack temperature, and dry/wet $H_2$ condition ($T_{hum}$) regardless of small (2-cell)/large cell (7-cell) stacks under the cases studied herein.

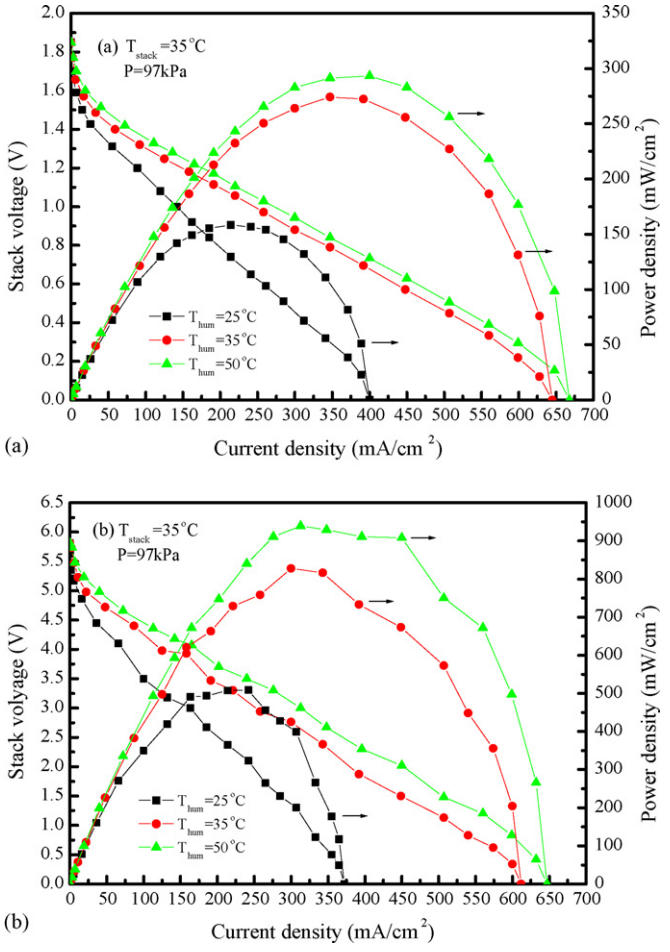


Fig. 11. The performance test for 2-cell stack and 7-cell stack at fixed $T_{stack}$ = 35 °C, $P$ = 97 kPa and different anode humidifier temperature. (a) 2-Cell stack. (b) 7-Cell stack.

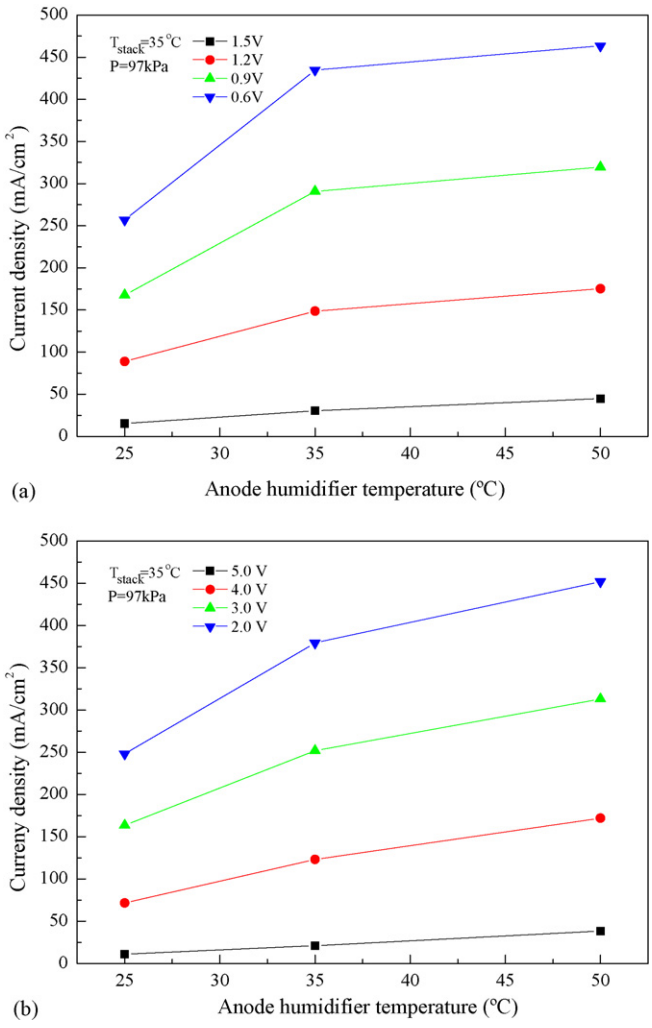


Fig. 12. Variation of current density for 2-cell stack and 7-cell stack at different stack voltage and anode humidifier temperature. (a) 2-Cell stack. (b) 7-Cell stack.

### 3.4. Stack reactant feed configurations

$H_2$ gas and air supply based on the present BPs design have their own delivering system. In PEM fuel cell stack, the method of reactant distribution to individual cells is also of great importance. $H_2$ gas and air were fed in series for the present study. The serial configuration forces a reactant feed and product removal flow stream from one cell to another cell in series. Higher pressure drop is expected as a result of the longer travelling length for the stream. The reactant distribution is normally not uniform from cell to cell along the reactant feed path evidenced by the present 7-cell stack VI and PI performance curves in ohmic polarization region shown in Figs. 6–8 except for small stack outcome in which the VI and PI curves exhibited similar results to those of single PEM fuel cells. In fact, the present 2-cell stack results of OCV are very close two-fold of the value for a single cell with nearly the same limiting current density. Such situation becomes a little changed as the number of cell increases in which a lower OCV and lower limiting current density are expected due to possibly uneven flow distribution of reactants to each cell.

## 4. Conclusions

For the first time, a micro PEM fuel cell stack with copper metal bipolar plates (BPs) was developed and tested with operational parameters. In-house-made 2-cell and 7-cell stacks with a cross section of 5 cm$^2$ and thickness of about 3.05 and 10.05 mm, respectively, used for the study. The operational parameters include the stack temperature, anode back-pressure, and the anode gas humidification temperature. The major results can be drawn as follows:

1. A low cost and high-mass production with high stack performance (250 mW cm$^{-2}$ at 0.8 V for 2-cell) at stack temperature of 25 °C has been fabricated and tested.
2. With humidified $H_2$ gas, the stack polarization showed only two stages. It seems that no mass transport process took place; however, this situation does not happen for dry $H_2$ condition.
3. The effect of operational parameters on stack performance seems similar to that of single cell in both trend and magnitude.

4. Stack reactant feed configuration indicates that the present in series fed for 2-cell stack is more suitable than that for 7-cell stack. The reasons caused this difference seems due to the uniformity of the reactant feeding. In spite of the deficiency, the present 2-cell and 7-cell stack results still show a reasonable performance.
5. Based on the present study for short-term stack performance, copper metal can be considered as one of the promising and powerful BP material candidates as far as the performance and cost are concerned if the weight and chemical activation can be reduced/or if these two factors are not important.

## Acknowledgment

This work was supported by National Science Council (NSC), Taiwan, ROC, under the contract number (NSC94-2218-E-110-004).

## References

[1] S.S. Hsieh, J.K. Kuo, C.F. Hwang, H.H. Tsai, Microsyst. Technol. 10 (2004) 121–126.
[2] S.S. Hsieh, C.F. Hwang, J.K. Kuo, H.H. Tsai, S.H. Yang, J. Solid State Electrochem. 9 (2005) 121–131.
[3] K.G. Stanley, E.K. Czyzewska, P.K. Vanderhoek, L.Y. Fan, K.A. Abel, Q.M. Wu, M. Parameswaran, J. Micromech. Microeng. 15 (2005) 1979–1987.
[4] S.H. Chan, N.T. Nguyen, Z. Xia, Z. Wu, J. Micromech. Microeng. 15 (2005) 231–236.
[5] S.S. Hsieh, J.K. Kuo, S.H. Yang, C.F. Huang, H.H. Tsai, Energy Convers. Manage. 47 (2006) 1868–1878.
[6] R. Eckl, W. Zehtner, C. Leu, U. Wagner, J. Power Sources 138 (2004) 137–144.
[7] L.J. Bonville, H.R. Kunz, Y. Sang, A. Mientek, M. Williams, A. Ching, J.M. Fenton, J. Power Source 144 (2005) 107–112.